JARO
Journal of the Association for Research in Otolaryngology

Research Article

Characterization of Stapes Anatomy: Investigation of Human and Guinea Pig

JAE HOON SIM,[1] CHRISTOF RÖÖSLI,[1] MICHAIL CHATZIMICHALIS,[1] ALBRECHT EIBER,[2] AND ALEXANDER M. HUBER[1]

[1]Department of Otorhinolaryngology, Head and Neck Surgery, University Hospital Zurich, Frauenkliniksrasse 24, 8091 Zurich, Switzerland
[2]University of Stuttgart, Stuttgart, Germany

ABSTRACT

The accuracy of any stapes model relies on the accuracy of the anatomical information upon which it is based. In many previous models and measurements of the stapes, the shape of the stapes has been considered as symmetric with respect to the long and short axes of the footplate. Therefore, the reference frame has been built based upon this assumption. This study aimed to provide detailed anatomical information on the dimensions of the stapes, including its asymmetries. High-resolution microcomputed tomography data from 53 human stapes and 11 guinea pig stapes were collected, and their anatomical features were analyzed. Global dimensions of the stapes, such as the size of the footplate, height, and volume, were compared between human and guinea pig specimens, and asymmetric features of the stapes were quantitatively examined. Further, dependence of the stapes dimensions on demographic characteristics of the subjects was explored. The height of the stapes relative to the footplate size in the human stapes was found to be larger than the corresponding value in guinea pig. The stapes showed asymmetry of the footplate with respect to the long axis and offset of the stapes head from the centroid of the medial surface of the footplate for both humans and guinea pigs. The medial surface of the footplate was curved, and the longitudinal arches of the medial surface along the long axis of the footplate were shaped differently between humans and guinea pigs. The dimension of the footplate was gender-dependent, with the size greater in men than in women.

Keywords: anatomy, footplate, guinea pig, human, microcomputed tomography (micro-CT), stapes

INTRODUCTION

The dimensions of the middle-ear ossicles have been studied using light microscopy (Sarrat et al. 1992; ÀWengen et al. 1995; Farahani and Nooranipour 2008), histological sections (Iyer and Gristwood 1984; Nadol 2001; Merchant et al. 2001), and microcomputed tomography (micro-CT) (Hagr et al. 2004; Elkhouri et al. 2006; Sim and Puria 2008). The resolution of the image in most studies using histological sections and micro-CT images is in the range of 10–20 µm, and the best resolution has been reported in studies by Elkhouri et al. (5.5 µm, gerbil middle ear) and Hagr et al. (6 µm, human middle ear). These studies have focused on the height of the stapes, the angle of the crura, and the area of the footplate. However, a detailed analysis of the symmetry of the stapes footplate has not been performed.

The input to the cochlea is defined by the motion of the stapes footplate. It has been known for several years that the motion of the stapes footplate in human (Hato et al. 2003; Sim et al. 2010a) and cat (Decraemer et al. 2000) is complex in the high frequencies. The stapes moves not only in a piston-like but also in a rocking-like manner, which includes rotational motions along the long and short axes of

Correspondence to: Jae Hoon Sim · Department of Otorhinolaryngology, Head and Neck Surgery · University Hospital Zurich · Frauenkliniksrasse 24, 8091 Zurich, Switzerland. Telephone: +41-44-2553680; fax: +41-44-2554164; email: JaeHoon.Sim@usz.ch

the stapes footplate. It has been shown that complex stapes motion elicits a hearing sensation in guinea pigs (Huber et al. 2008; Eiber et al. 2012). The exact mechanism of the hearing sensation is not fully understood because an associated fluid motion has not been measured. Further, it remains unclear which characteristics of the stapes anatomy of guinea pigs contribute to the hearing sensation and whether these findings can be directly applied to humans.

In order to investigate the effects of stapes motion on cochlear fluid displacement and, thus, hearing, numerical models have been developed (Eiber 1999; Koike et al. 2002; Gan et al. 2007). The accuracy of these models relies on the accuracy of the information they are based on. Though the three-dimensional (3-D) volume of the stapes constructed from the histological sections of micro-CT images actually includes asymmetrical features, the asymmetrical features have not been systemically quantified. Further, in most existing numerical models, the stapes has been simplified to have symmetric shapes and dimensions between the anterior and posterior parts and between the superior and inferior parts. In addition, the medial surface of the footplate, which interfaces with the cochlear fluid, is modeled as a flat surface, indicating negligible effects on fluid flux in the cochlea of the in-plane motion of the stapes along the footplate plane. With the assumption of the flat medial surface, in-plane motion of the stapes causes only shear stress on the cochlear fluid. According to a classical theory of viscous flow, the fluid flow by the shear stress is presumed to be much smaller than the fluid flow by the normal stress caused by out-plane motion (i.e., piston-like and rocking-like motions) of the stapes. Such assumptions may be different from the real shapes of the stapes. Therefore, modeling of the stapes requires that the anatomic information be comprehensive and as accurate as possible. Further, the exact dimensions of the stapes are also necessary for the development of active and passive middle-ear prostheses.

Differences in middle-ear anatomy between humans and guinea pigs have been observed in previous studies. The lever ratio in the "hinging" motion of the malleus–incus complex, which is defined as the ratio of the vertical distance between the rotational axis and the umbo to the vertical distance between the rotational axis and the incus tip, is about 1.3 for human ears (Rosowski and Merchant 1995), while the ratio in guinea pig ears is more than 2 (Puria et al. 2007; Puria and Steele 2010). Further, according to Puria et al. and Puria and Steele, while guinea pig ears have fused malleus–incus complexes with their eardrum's symmetry in the anterior and posterior areas, the malleus–incus joint is flexible and the eardrum is asymmetric in its anterior

and posterior areas in human ears. They argued that such features of human middle ears may be adaptive to a "twisting" mode of the malleus motion along the superior–inferior axis of the malleus to overcome large magnitudes of middle-ear inertia at high frequencies. As the anatomical features and motions of the middle ear are different between human and guinea pig ears, the stapes of the two species are also expected to have structural differences.

Detailed information on the dimensions of the stapes can be obtained using several techniques, for example, observation and measurements using microscopes, histological sections, orthogonal plane fluorescence optical sectioning (OPFOS), magnetic resonance microscopy (MRM), or micro-CT. Observation via microscopes can provide a good overview, but it might not be the most precise way of measuring the dimensions of the ossicles. Estimates of the dimensions of the ossicles based on histological sections are precise; however, artifacts that occur during preparation of the slides may appear. The OPFOS requires elaborate preparation, including decalcification (Voie et al. 1993; Decraemer et al. 2003; Buytaert et al. 2011), and such preparation may not be necessary when only measuring the bony structures of the stapes. The MRM can be used to obtain the anatomy of the middle-ear ossicles (MRM image data of several mammals are available at http://www-cellbio.med.unc.edu/henson_mrm/), but the tympanic space should be filled with fluid for the MRM imaging of the middle ear (Lane et al. 2005). An accurate and efficient method for measuring the bony structures of the stapes is to use micro-CT, which allows 3-D reconstruction. The accuracy of this technique is increasing, and its value has been reported (Sim and Puria 2008). Therefore, this technique was chosen for this investigation.

The aims of this study were to (1) describe a precise method for dimensional analysis of the structure of the stapes, (2) compare the results of this study with the results in the literature, (3) use the method in both human and guinea pig and evaluate the results in terms of the effects that the anatomical features have on the rocking-like motions of the stapes and reliability of the measurement of stapes spatial motion, and (4) investigate whether demographic characteristics, such as gender, body weight, body height, or brain weight, correlate with stapes dimensions in humans.

MATERIAL AND METHODS

Collection of the stapes

Micro-CT images of 53 stapes from 53 human temporal bones (TBs) and 11 stapes from 11 female guinea pigs were used for this study. The human TBs

were from subjects who died in the University Hospital Zurich from 2008 to 2011, and the exclusion criteria for the human TBs for this study were osseous fracture and otosclerosis of the stapes. Most of the human stapes were from the right side (51 of the 53). Because the human TBs had usually been used for other experiments, the whole structure of the stapes was available in only 32 of the 53 and only the footplate and partial crura were available in 21 of the 53. Subject information of the humans from which the TBs were extracted was recorded for 40 of the 53 (19 for the intact stapes and 21 for the footplate and partial crura). The average age of the 40 human subjects was 60.9 years, with a standard deviation of 13.7 years. The subject information also included gender, body weight, body height, and brain weight. The guinea pigs were in the same age, weight class, and family. Ten of the 11 guinea pig stapes were from the right side, and all of the guinea pig stapes were intact.

Micro-CT imaging and 3-D reconstruction

The specimens were imaged using the µCT 40 or µCT 100 (SCANCO Medical AG, Switzerland). Most human stapes and all the guinea pig stapes were imaged with other ear structures by µCT 40, which has 8 µm as its best achievable resolution. When the stapes was scanned with other ear structures, the achievable resolution was determined by the size of the prepared specimen. The obtained resolution (size of the isotropic voxel) was 10.5 or 15 µm. As this study focused on anatomical features of the stapes, the features of the other ear structures were not included in this study. The µCT 100, which could achieve a resolution (size of the isotropic voxel) of 5 µm, was used only for four dissected human stapes. The resolution of 10.5 or 15 µm with µCT 40 showed little difference from the 5-µm resolution with µCT 100 for bony structures of the stapes, which were clearly distinguished from ambient soft tissues and air. The X-ray intensity and the photon energy level were set to 145 µA and 55 keV, respectively, to obtain good image quality (Sim et al. 2007; Sim and Puria 2008). The specimen was wrapped to avoid drying during the micro-CT scan.

Segmentation and 3-D volume reconstruction were performed using the *Evaluation Program*, which was built-in and was provided by the micro-CT manufacturer. First, the stapes was separated from ambient air and peripheral structures by an outline contour in each slice image. The outline contours were initially drawn by hand and adjusted to the edge of the bony structure of the stapes by a "shrink–wrapping" algorithm in the *Evaluation Program*. Next, the grayscale range of 300–1,000, where the maximum attenuation (i.e., the mass attenuation coefficient μ/ρ equals to 8 cm^2/g, Johns and Cunningham 1974; Macovski

1983) corresponds to 1,000 and no attenuation ($\mu/\rho=0$) corresponds to 0, was selected for the bony parts of the stapes. Figure 1 displays the segmented bony parts of the human stapes on a slice image, for a scan with the 10.5-µm resolution (A) and with the 5-µm resolution (B). After segmentations were done for a stack of slices, the segmented slices were combined to reconstruct the 3-D volume of the stapes. The 3-D volume data were stored in AIM file format, which is a specific binary format for the *Evaluation Program* containing a user-defined nonzero value for pixels of the selected bony parts and zero for other pixels. In addition to the 3-D volume data, a surface model of the stapes was generated in the Standard Tessellation Language (STL) file format for dimensional analysis of the stapes structures.

Intrinsic frame of the stapes

As the medial surface interfaces the cochlear fluid and the motion of the medial surface determines stimuli to the cochlea, a frame based on the geometry of the medial surface of the stapes footplate was defined as an intrinsic frame. A plane was obtained such that the sum of the squared distances from the plane to points on the medial surface of the footplate was minimized and was set as the *x–y* plane. The centroid of the surface was taken as the origin of the frame. Consequently, the *z*-axis was normal to the plane and the lateral direction was set to its positive direction. On the *x–y* plane, the *x*-axis was aligned along the long axis and the *y*-axis was aligned along the short axis of the footplate. As the orientations of the long and short axes of the footplate were not accurately identified in the real shapes of the footplate, they were assigned such that the ratio of the length along the short axis to the length along the long axis was the minimum. The anterior and superior directions were taken as the positive directions for the *x*- and *y*-axes, resulting in a right-handed frame system for the right ear and a left-handed frame system for the left ear. The surface model in STL format was imported to a commercial software, Rapid-Form XOS2 (3D Systems Corp., Korea). Calculation of the intrinsic frame and registration of the surface model into the constructed frame were also done by the RapidForm XOS2. Only the calculation for the fine adjustments of the *x*- and *y*-axes on the *x–y* plane was done using a custom-made Matlab (The Math-Works Inc., USA) code.

Principal frame of the stapes

In addition to the intrinsic frame based on the medial surface of the stapes footplate, the principal frame, which consists of the principal axes with the center of
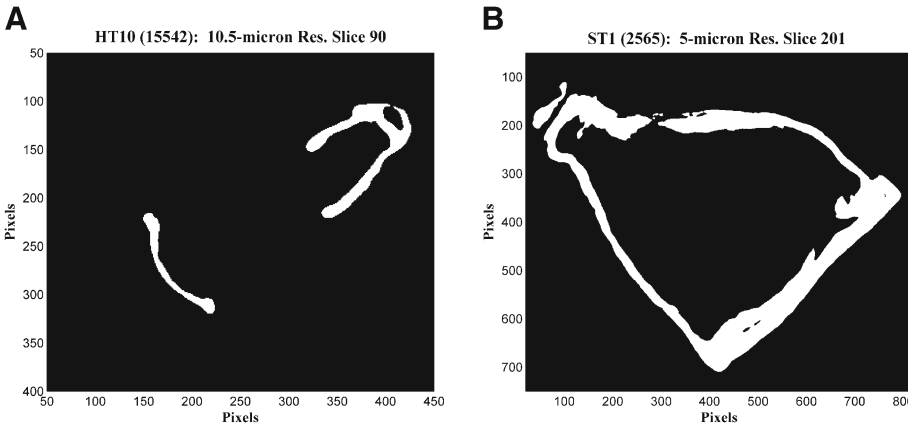
A

HT10 (15542): 10.5-micron Res. Slice 90

B

ST1 (2565): 5-micron Res. Slice 201

FIG. 1. Segmented bony parts of the human stapes on a slice image for scans **A** with the 10.5-μm resolution and **B** with the 5-μm resolution. The *white parts* represent the selected bony parts and *numbers on the axes* indicate the numbers of the pixels. The same grayscale range of 300–1,000 (1,000 is the maximum attenuation and 0 is no attenuation) was selected for both the scan resolutions.

mass as its origin and thus is characterized by inertial properties of the stapes, was calculated as another reference frame (Sim et al. 2007, 2010a, b). While the intrinsic frame was constructed based on surface features of the medial side of the stapes footplate, the principal frame was calculated from 3-D volume data in AIM format (see the "Micro-CT imaging and 3-D reconstruction" section). A custom-made Matlab code was used for the calculation of the principal frame.

Though both the high-density bony parts and the low-density blood vessels were included in the calculations of the principal frames of the malleus and incus in studies by Sim et al. and Sim and Puria, only the high-density bony parts were considered with a uniform density for calculation of the principal frame in this study. The low-density parts of the blood vessels were rarely seen for the stapes because of the relatively thin structures; therefore, considering only the high-density bony parts was expected to cause negligible errors. The corresponding principal moments of inertia (PMOIs) could not be obtained because the mass of the stapes was not measured. Instead, since the density of the stapes is a common factor for the PMOIs and mass of the stapes, the ratios of the three PMOIs to the mass of the stapes could be calculated.

Measurement of stapes dimensions

Anatomical dimensions of the stapes were measured with the stapes registered into its intrinsic frame, using built-in functions in the RapidForm XOS2. Figure 2 represents references for the stapes dimensions with symbols. First, the total volume V_{ST} and height h of the stapes were measured. The height was defined as the distance from the center of the stapes head's surface, which joins to the lenticular process, to the plane fitting to the medial surface of the footplate (i.e., x–y plane). For the dimensions of the stapes footplate, lengths a along the long axis and b along the short axis and area of the medial surface A_{FT} were measured. For comparison between the height of the stapes and the area of the footplate, which have

different units, the equivalent diameter d_{eq} of the stapes footplate was defined by and calculated using:

$$\frac{\pi}{4} d_{eq}^{2} = A_{FT} \tag{1}$$

The shape of the stapes was characterized by several ratios between the measured lengths: a/b for the shape of the stapes footplate, h/d_{eq} for the height relative to the footplate size, and h_c/h for the location of the center of mass relative to the height. h_c indicates the height of the center of mass as the distance from the center of mass to the medial surface plane (i.e., x–y plane). The profile of the medial surface of the footplate was also obtained, and the distance of each point on the medial surface from the x–y plane was taken as the deviation of the point from the x–y plane.

Asymmetric shapes of the stapes footplate were examined and quantified in the intrinsic frame. Length from the centroid of the medial surface of the footplate (i.e., the origin of the intrinsic frame) to the anterior edge of the footplate through the long axis (i.e., x-axis) was defined as the anterior length a_{ant} and was compared to the posterior length a_{pos}, which was defined as the length from the origin to the posterior edge. Similarly, the superior and inferior lengths were defined as lengths along the short axis (i.e., y-axis) and were compared with each other. These references for asymmetric features of the footplate are shown in Figure 3. In addition, the outline of the footplate is shown in the x–y plane (red in Fig. 3) to see the diversity of the outlines across the TBs. Deviation of the stapes head was characterized by the amount and direction of the deviation from the z-axis of the intrinsic and principal frames. Orientation of the principal frame relative to the intrinsic frame was also examined.

The thickness of the footplate was measured along the annular rim of the footplate. For this measurement, the annular rim was separated (red in Fig. 2B)
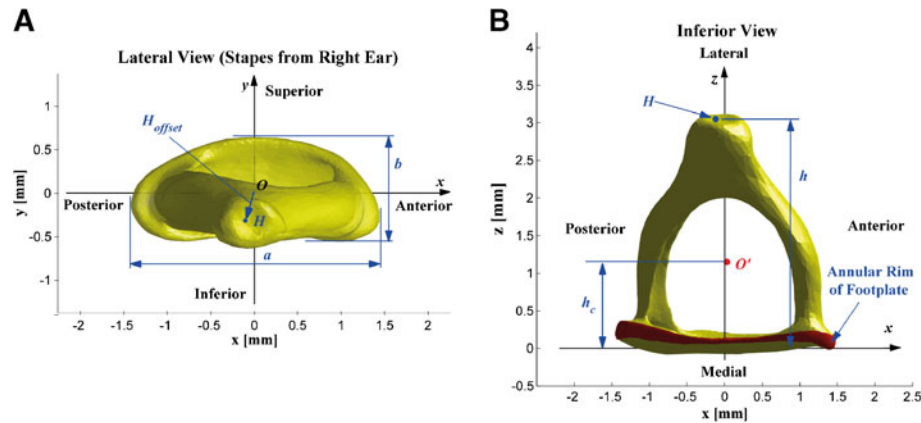
FIG. 2. References for the stapes dimensions. **A** Lateral view and **B** inferior view. *a* long length of footplate, *b* short length of footplate, *h* total height of the stapes, h_c height of the center of the mass. Other references not shown in the figure are as follows: A_{FT} footplate area (medial surface), A_{FT_proj} projected footplate area (to *x–y* plane), d_{FT_eq} equivalent diameter of the footplate area, $d_{FT\_eq\_proj}$ equiva-

lent diameter of the projected footplate area, V_{ST} volume of the stapes. *H* represents the centroid of the stapes head surface with an offset from the origin *O* of the intrinsic frame (H_{offset}) and *O'* represents the center of mass of the stapes. The annular rim of the footplate is shown in *red*.

Dependence of stapes shapes and dimensions on human subject characteristics

Dependence of shapes and dimensions of the stapes footplate on the characteristics of the subjects, including gender, age, height, body weight, and brain weight, was examined for 40 of the 53 subjects. Dependence of the volume and height of the stapes on the subject data was not examined due to the limited number of available data for both parameters (the whole structures of the stapes were available in 32 of the 53 stapes, and subject data were available in 19 of those 32 stapes).
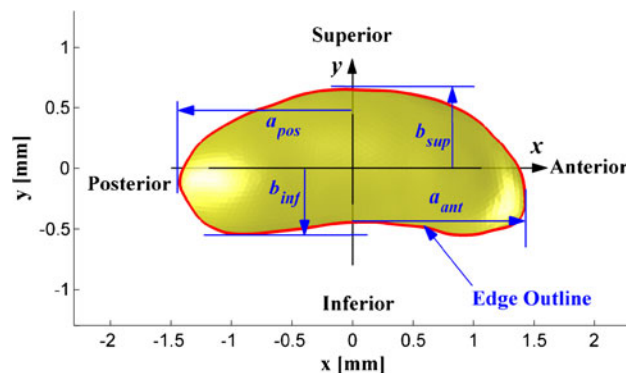

FIG. 3. References for the asymmetry of the stapes footplate. The outline of the footplate (*red*) was also obtained to diversity of the outline shape across the TBs.

Statistical calculation

All dimensions of the stapes were averaged across the TBs and were represented in the form of mean value± standard deviation.

The Mann–Whitney test was used for comparison of anatomical dimensions and shapes between human and guinea pig. The Mann–Whitney test was also applied to comparison of the stapes dimensions between the data from male and female human subjects. Significance of the asymmetrical features was assessed using the Wilcoxon signed-rank test. Linear regression was used to examine the correlation between the dimensions of the stapes and human subject data.

All statistical calculations were performed using InStat V3.1 software (GraphPad Software Inc., La Jolla, CA, USA). *p* values of <0.05 (two-tailed) were considered to be significant, and the levels of significance were classified into three groups of <0.05, <0.01, and <0.001.

RESULTS

Two reference frames and ratios between principal moments of the inertia

Figure 4 displays the relative positions of the three principal axes in the intrinsic reference frame (*n*=28 for human stapes and *n*=9 for guinea pig stapes). The principal axis with the minimum principal moment of inertia was in the medial–lateral direction (*z'*-axis), the principal axis with the middle principal moment of inertia in the inferior–superior direction (*y'*-axis), and the principal axis with the maximum principal moment of inertia in the posterior–anterior direction (*x'*-axis) for both human and guinea pig stapes. In Figure 4, (x_1, y_1, z_1), (x_2, y_2, z_2), and (x_3, y_3, z_3) represent

Methods (continued)

and the thickness in the *z*-axis was measured at every 10 ° along the annular rim. As the thickness map showed similar trends, only three for each of the human and guinea pig stapes were examined.
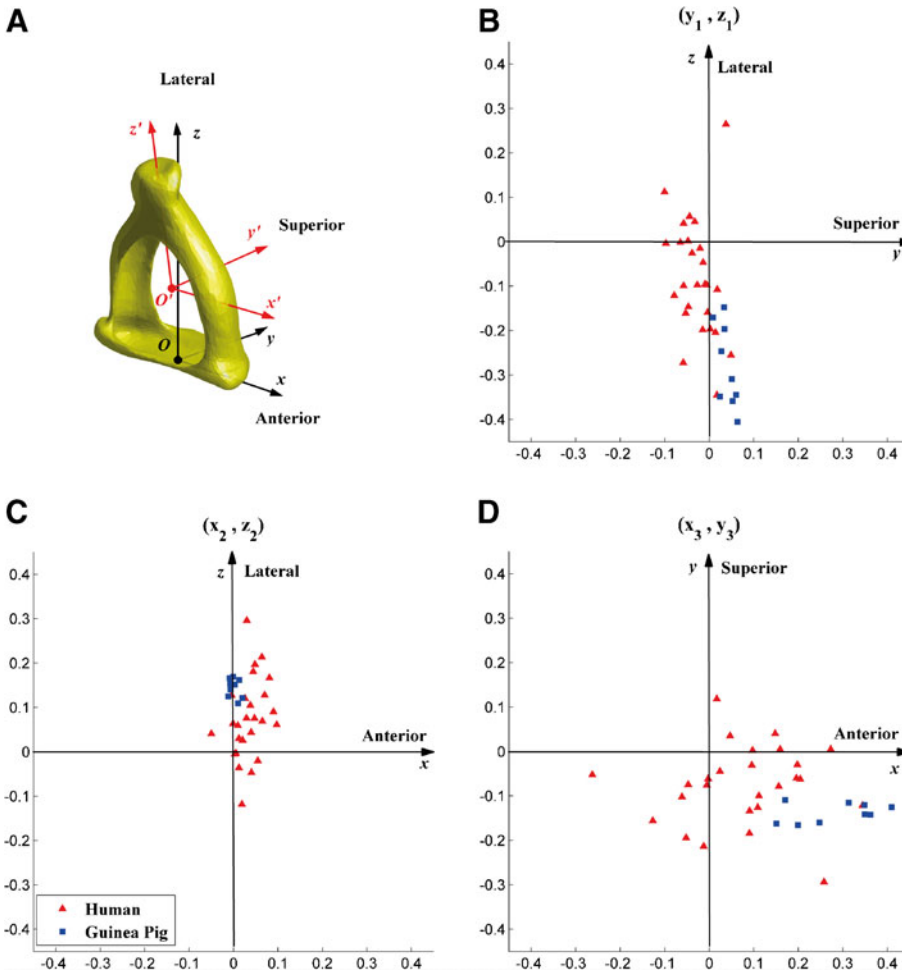
A

B

C

D

FIG. 4. Relative position of the three principal axes in the intrinsic reference frame ($n=28$ for human stapes and $n=9$ for human stapes. **A** Principal frame ($x'y'z'$, *red*) and the intrinsic frame (xyz, *black*) in a human stapes, **B** position of x'-axis relative to x-axis, **C** position of y'-axis relative to y-axis, and **D** position of z'-axis relative to z-axis. (x_1, y_1, z_1), (x_2, y_2, z_2), and (x_3, y_3, z_3) represent coordinates of the unit vectors of the x'-, y'-, and z'-axes, respectively, in the intrinsic frame.

coordinates of the unit vectors of the x'-, y'-, and z'-axes, respectively, in the intrinsic frame. The x'-axis was tilted toward the lateral direction from the x-axis (Fig. 4B) and the y'-axis was tilted toward the medial direction from the y-axis of the intrinsic frame (Fig. 4C) in both the human and guinea pig stapes. The z'-axis was always tilted toward the anterior–inferior direction from the z-axis in the guinea pig stapes and was generally toward the inferior direction in the human stapes (Fig. 4D). The angle between the z-axis and z'-axis was 10.0 ± 4.98 ° for human and 18.6 ± 4.52 ° for guinea pig.

Table 1 lists the ratios (mean±standard deviation) of the three PMOI ($I_{x'x'}$, $I_{y'y'}$, and $I_{z'z'}$ in x'-, y'-, and z'-

axes, respectively) to the mass of the stapes m_{ST}. The ratio for the x'-axis was larger than the ratio for the y'-axis by factors of 1.36 ± 0.073 for human stapes and 1.48 ± 0.025 for guinea pig stapes. The ratio for the x'- and z'-axes in the guinea pig stapes was larger than the corresponding ratio in the human stapes ($p<0.05$ and $p<0.001$, respectively, with the Mann–Whitney test).

Overall dimensions

Table 2 lists the means and standard deviations for the measured dimensions of the stapes. The projected

TABLE 1

Ratios (mean±standard deviation) of the three PMOIs ($I_{x'x'}$, $I_{y'y'}$, and $I_{z'z'}$ in x'-, y'-, and z'-axes, respectively) to the mass of the stapes m_{ST}

Description	Symbol	Human	Guinea pig	p value[a]
PMOI in x'-axis/mass of the stapes	$I_{x'x'}/m_{ST}$ [g/m]	1.35±0.191	1.56±0177	< 0.05
PMOI in y'-axis/mass of the stapes	$I_{y'y'}/m_{ST}$ [g/m]	1.00±0.150	1.05±0.113	0.336
PMOI in z'-axis/mass of the stapes	$I_{z'z'}/m_{ST}$ [g/m]	0.47±0.082	0.71±0.082	< 0.001

The Mann–Whitney test was applied to the comparison between the human and guinea pig. $n=28$ for human and $n=9$ for guinea pig

[a] p values represent the significance of the differences between human and guinea pig stapes

Dimensions (mean±standard deviation) of the stapes in humans and guinea pigs

Description	Symbol	Human	Guinea pig
Long length of footplate	a [mm]	2.81±0.158	1.44±0.034
Short length of footplate	b [mm]	1.27±0.109	0.66±0.029
Long length/short length of the footplate	a/b	2.22±0.197	2.19±0.092
Footplate area (medial surface)	A_{FT} [mm^2]	3.03±0.331	0.79±0.039
Projected footplate area (to x–y plane)	A_{FT_proj} [mm^2]	2.86±0.316	0.76±0.034
Projected footplate area/footplate area	A_{FT_proj}/A_{FT}	0.94±0.015	0.97±0.007
Equivalent diameter of the footplate area	d_{FT_eq} [mm]	1.96±0.108	1.00±0.024
Equivalent diameter of the projected footplate area	$d_{FT\_eq\_proj}$ [mm]	1.90±0.106	0.98±0.022
Volume of the stapes	V_{ST} [mm^3]	1.43±0.242	0.19±0.017
x-coordinate of the center of the mass	x_c [mm]	0.001±0.091	−0.002±0.011
y-coordinate of the center of the mass	y_c [mm]	−0.116±0.085	−0.043±0.026
Height (z-coordinate) of the center of the mass	h_c [mm]	1.22±0.157	0.40±0.033
Total height of the stapes	h [mm]	3.28±0.210	1.33±0.039
Height of the center of the mass/total height	h_c/h	0.37±0.041	0.30±0.027
Total height/equivalent diameter of the footplate	$h/d_{FT\_eq\_proj}$	1.72±0.123	1.35±0.042

$n=53$ (footplate dimensions) or $n=32$ (other dimensions) for human and $n=11$ for guinea pig

area of the medial surface of the footplate was 94±1.5 % (human) and 97±0.7 % (guinea pig) of the non-projected surface area. The ratio of the long length a to the short length b of the footplate was similar for human and guinea pig. However, the relative ratio of the stapes height to the equivalent diameter of the footplate $h/d_{FT\_eq\_proj}$ in the human stapes (1.72±0.123) was larger than the corresponding ratio in the guinea pig stapes (1.35±0.042), and the difference was significant ($p<0.001$ with the Mann–Whitney test). The center of mass in the human stapes was located slightly more laterally than the center of the mass in the guinea pig stapes (h_c/h was 0.37±0.041 for human and 0.30±0.027 for guinea pig). The center of mass of the stapes had an offset toward the inferior direction in both human and guinea pig (y-coordinate of the center of mass was −0.116±0.085 in human and −0.043±0.026 in guinea pig). Relative individual differences (i.e., the standard deviations divided by the corresponding mean values) in the stapes dimensions were generally larger in human than in guinea pig, showing larger standard deviations.

Medial surface of the footplate

Figures 5 and 6 represent surface profiles of the medial surface of the footplate for a human stapes and a guinea pig stapes, respectively. The longitudinal (B) and transverse (C) arches of the medial surface were obtained along the long axis (x-axis) and short axis (y-axis) of the footplate from 29 human stapes and 11 guinea pig stapes. In most of the human stapes, the longitudinal arch was concave medially around the origin and convex medially in the anterior and posterior parts (Fig. 5B). The curvature of the averaged longitudinal arch was approximately 0.25 mm^{-1} around the origin (C_{HLO}) and approximately 0.30 and 0.65 mm^{-1} in the convex regions of the anterior (C_{HLA})

and posterior (C_{HLP}) parts, respectively. The transverse arch of the medial surface along the short axis (y-axis) in the human stapes was convex medially (Fig. 5C), and the curvature was 0.75 mm^{-1} (C_{HT}). The surface generally had its peak in the anterior part of the surface and its deepest depression in the superior and inferior parts. In the guinea pig stapes shown in Figure 6B, C, both the longitudinal and transverse arches of the medial surface were convex medially with their peaks near the centroid of the surface. The curvature of the averaged longitudinal (C_{GL}) and transverse (C_{GT}) arches was 0.55 and 1.10 mm^{-1}, respectively.

The distance between the peak and the deepest depression of the surface (D_{off} in Figs. 5D and 6D) was 0.24±0.035 mm (mean±standard deviation) for human and 0.15±0.014 mm for guinea pig. Considering the size of the footplate of the human and guinea pig, the distance between the peak and the greatest depression was similar ($D_{off}/d_{FT\_eq\_proj}$ was 0.13±0.017 for human and 0.15±0.014 for guinea pig).

A shape like a big toe (circled area in Fig. 5A), which was protruding toward the medial direction at the anterior–inferior edge, was observed in 29 of the 53 human stapes, and it was not observed in guinea pigs.

While the distinguishable patterns of the surface profile between human and guinea pig were generally maintained in other human and guinea pig stapes, some differences across the human TBs were observed. Four types of medial surface which were different from the general profiles for the human stapes are appended (see Fig. 11 of the Appendix).

Asymmetry of the stapes dimensions

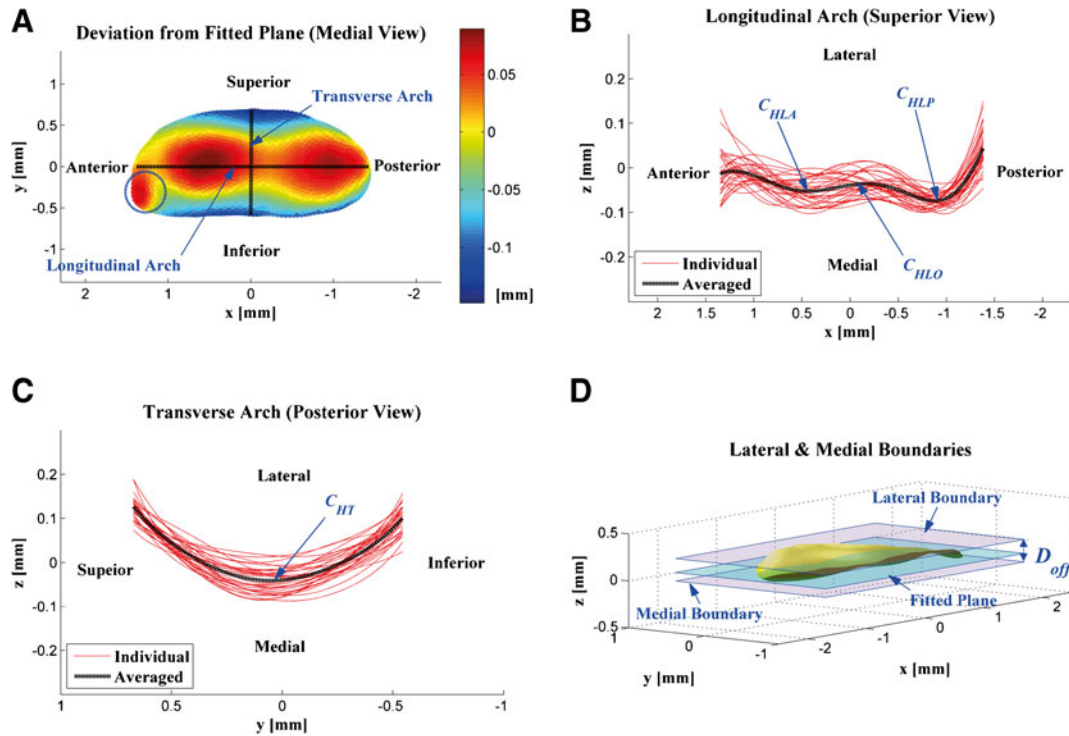Figure 7 illustrates outlines of the medial surface of the footplate (corresponds to red in Fig. 3) on the x–y

FIG. 5. Surface profiles (medial surface) of the footplate in the human stapes. **A** Deviation from the fitted plane (x–y plane), **B** longitudinal arch of the medial surface along the long axis (x-axis), **C** longitudinal arch of the surface along the short axis (y-axis), and **D** lateral and medial boundary of the surface. The longitudinal and transverse arches were obtained from 29 human stapes, and average arches were calculated.

plane in the human (left, $n=53$) and guinea pig (right, $n=11$) stapes.

Table 3 describes the asymmetric features of the stapes footplate quantitatively. While the anterior length a_ant and posterior length a_pos of the footplates were similar, the superior b_sup and inferior b_inf lengths showed significant differences ($p<0.001$) in both human and guinea pig. The superior length was larger than the inferior length by factors of 1.15 ± 0.072 (mean±standard deviation, human) and 1.17 ± 0.044 (guinea pig).

As another measure of the asymmetry of the stapes, the location of the centroid of the stapes head (H; Fig. 2) relative to the origin was examined in the intrinsic and principal frames. Figure 8 illustrates the offset of the stapes head from the origin in the intrinsic frame (A) and in the principal frame (B). To represent the relative amounts of offsets in both frames, the x- and y-coordinates of the centroid of the stapes head were normalized by the z value. In the intrinsic frame, the centroid of the head of the guinea pig stapes was offset in the anterior–inferior direction. The centroid of the human stapes head also showed a similar trend. In the principal frame, while the centroid of the human stapes head was distributed around the origin, the centroid of the guinea pig stapes head was offset to the posterior direction.

Figure 9 illustrates the thickness map of the annular rim of the footplate for three human and guinea pig

stapes. The relative magnitudes of the averaged thickness are shown with different-sized circles at the corresponding locations (upper figures), and individual measurements are shown (figures in the bottom) for the human (A) and guinea pig (B) stapes. While the three thickness distributions in each of human and guinea pig stapes showed similar trends, the thickness map of the human and guinea pig stapes showed distinguishable shapes. In the human stapes, the annular rim has the greatest thickness in the posterior region and the smallest thickness in the anterior region. In the guinea pig stapes, the thickness of the annular rim was almost constant along the whole superior region and the thickness in the inferior region was smaller than in the superior region.

Dependence of stapes shapes and dimensions on patient data in human

The dimensions of the stapes footplate showed a strong dependence on the gender of the subject (Table 4). While the long length of the footplate was not significantly different between female and male subjects, the short length of the footplate was significantly different, resulting in a significant difference of the footplate area as well. Consequently, the ratio of the long length of the footplate to the short length of the footplate in female subjects (2.35 ± 0.201 (mean±standard deviation)) was larger than the ratio
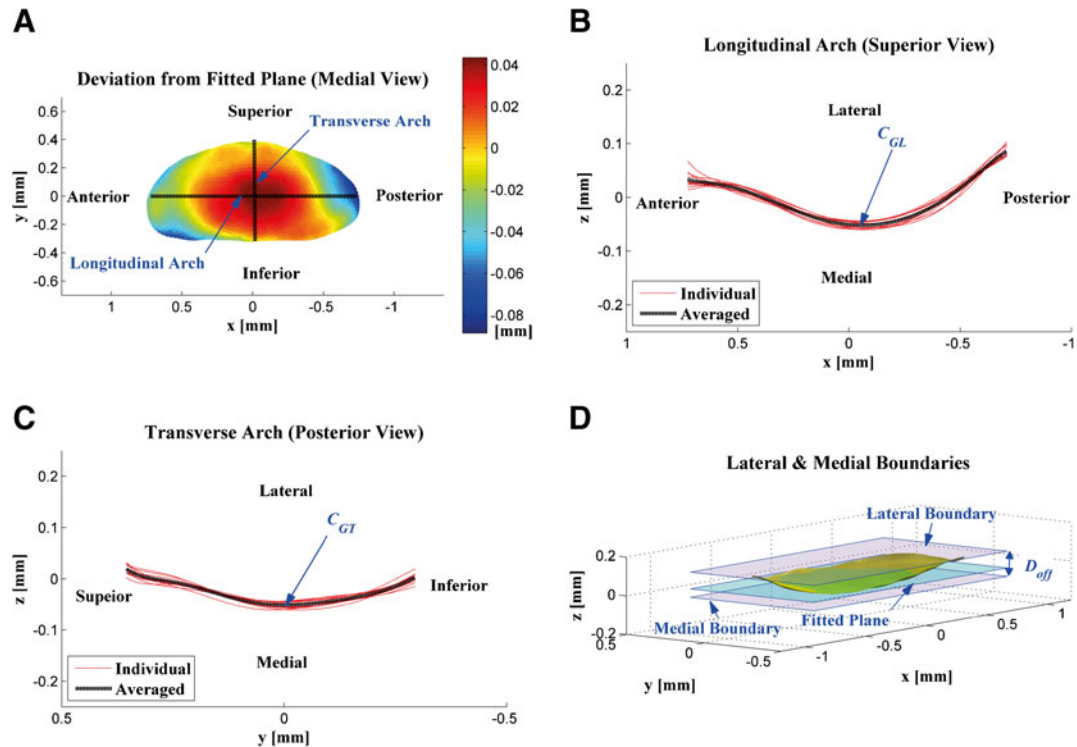
FIG. 6. Surface profiles (medial surface) of the footplate in the guinea pig stapes. **A** Deviation from the fitted plane (x–y plane), **B** longitudinal arch of the medial surface along the long axis (x-axis), **C** longitudinal arch of the surface along the short axis (y-axis), and **D** lateral and medial boundary of the surface. The longitudinal and transverse arches were obtained from 29 human stapes, and average arches were calculated.

in male subjects (2.14 ± 0.137). Though the mean difference was only 9.8 % of the mean value in female subjects, it was statistically significant ($p<0.001$ with Mann–Whitney test).

While the dimensions of the stapes footplate showed significant difference between female and male subjects, the total height of the stapes did not. As the total height of the stapes was available only for a limited number of subjects ($n=5$ for female and $n=14$ for male subjects), the statistical significance of the result was not computed.

The asymmetry of the footplate (i.e., a_{ant}/a_{pos} and b_{sup}/b_{inf}) in male subjects was greater than in female subjects, but the difference was small (only within 5 % of the corresponding values).

There was no correlation of the dimensions of the stapes footplate with other subject data, such as height, body weight, brain weight, and body mass index. As an

example, no correlation of the footplate area with age, height, body weight, or brain weight could be observed in Figure 10. Using linear regression, correlation of the footplate area with height, body weight, brain weight body, and mass index resulted in p values of 0.646, 0.184, 0.737, and 0.157, respectively.

DISCUSSION

Comparison of human data with other studies

Depending on the scope of the study (e.g., surgical or anatomical vs. mechanical), previous studies have focused on different parameters of the stapes dimensions. One purpose of this study was to use a precise technique to collect all potentially important values and combine them in one publication. Table 5 shows the comparison of the human stapes data in this study
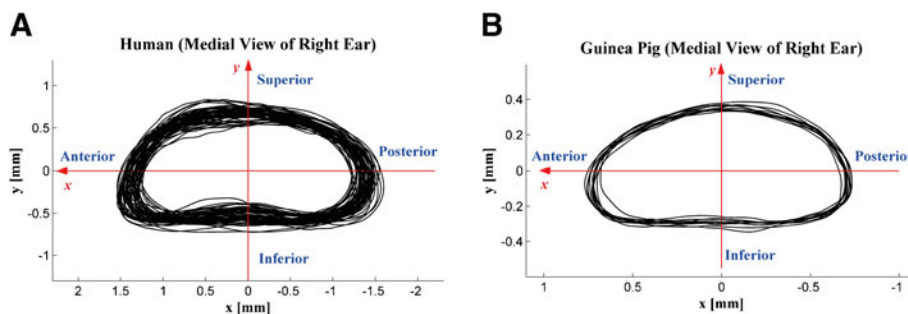

FIG. 7. Outlines of the medial surface of the footplate (corresponds to *red* in Fig. 3) on the x–y plane **A** in the human stapes ($n=53$) and **B** in the guinea pig stapes ($n=11$).

Asymmetry of the stapes footplate (mean±standard deviation)

Description	Symbol	Human	Guinea pig
Anterior length of the footplate	a_{ant} [mm]	1.41±0.087	0.73±0.027
Posterior length of the footplate	a_{pos} [mm]	1.40±0.086	0.71±0.017
Anterior/posterior length of the footplate	a_{ant}/a_{pos}	1.01±0.054	1.02 ±0.039
Significant difference between a_{ant} and a_{pos}	p value	0.186	0.083
Superior length of the footplate	b_{sup} [mm]	0.68±0.066	0.36±0.016
Inferior length of the footplate	b_{inf} [mm]	0.59±0.049	0.30±0.015
Superior/inferior length of the footplate	b_{sup}/b_{inf}	1.15±0.072	1.17±0.044
Significant difference between b_{sup} and b_{inf}	p value	< 0.001	< 0.001

Wilcoxon signed-rank test was applied to see significant differences between a_{sup} and a_{inf} and between b_{sup} and b_{inf}. $n=53$ for human and $n=11$ for guinea pig

with data reported in the literature. As our data were in good agreement with the literature, the methods that we used to define stapes dimensions are presumed to be reliable and valid. Some differences were observed in the projected area of the footplate (2.86± 0.316 mm^2 in this study and 3.00–5.30 mm^2 in a work by Stenfelt et al. 2004). Considering that Stenfelt et al. used photographs to measure the projected area of the footplate, we presume that our data are likely to be a more accurate representation. The large deviation across TBs in Stenfelt et al. (3.00 to 5.30 mm^2) was not observed in the 53 TBs. The footplate area (presented in Wever and Lawrence 1954, p. 417) and height (Wysocki and Sharifi 2005) of the guinea pig stapes were measured through optical views. The footplate area in this study (0.79±0.039 mm^2) was smaller than the area measured by Whittle (0.79 to 0.95 mm^2, with an average of 0.88 mm^2), and the height (1.33±0.039 mm) was larger than the height measured by Wysocki and Sharifi (1.12±0.17 mm).

According to Funnell (1984), an insufficient number of segments can result in a serious error in area calculation. In the work, it was suggested that the size of the segment (i.e., distance between adjacent vertices) should be similar to or smaller than the size of the distance between the slice images. That is, if the pixel size in slice images is considerably larger than the distance between the slice images, it will result in a large error in the area calculation. In this study, the isotropic voxels (i.e., the pixel size in slice images are identical to the incremental distance between the slice images) were used for the micro-CT scan. Then, when the STL files were generated using a built-in function of the *Evaluation Program* in this study, the same downscale factor of 2.0 (for guinea pig stapes) or 4.0 (for human stapes) was applied to all the three axes of the micro-CT frame. Therefore, the error of the area calculation in this study is presumed to be small.

Human vs. guinea pigs

One difference between the human and guinea pig stapes was that the height relative to the footplate size in the human stapes was larger than the corresponding value in guinea pig. The ratio of total height to the equivalent diameter of the footplate was 1.72±0.123 for human and 1.35±0.042 for guinea pig. The center of mass of the stapes was also closer to the footplate in guinea pig (h_c/h=0.30±0.027) than in human (h_c/h= 0.37±0.041). Effects of the ratio of the height to the footplate size on rocking-like motions of the stapes have two opposite aspects: first, stimuli for the rocking-like motions, and second, constraints for the rocking-like motions. When forces act in the x- and y-directions on the stapes head, they result in moments (torques) for the rocking-like motions of the stapes footplate (Huber
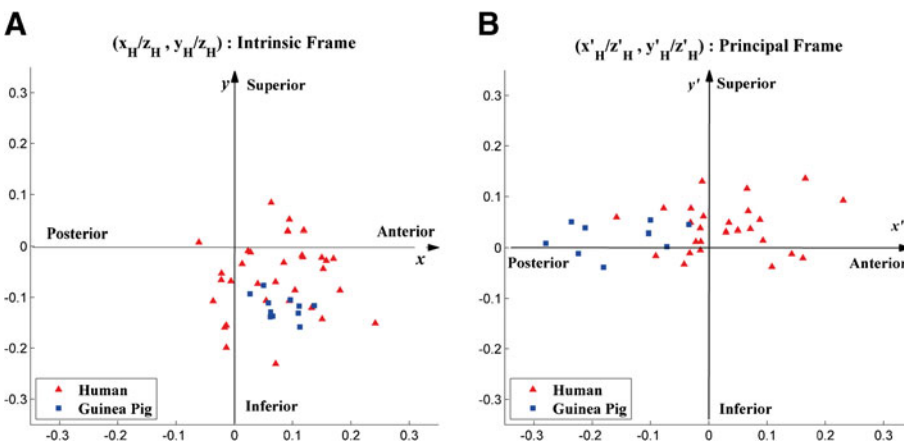

FIG. 8. Offset of the stapes head from the origin **A** in intrinsic frame ($n=32$ for humans and $n=11$ for guinea pigs) and **B** in principal frame ($n=28$ for humans and $n=9$ for guinea pigs). In the intrinsic frame, (x_H/z_H, y_H/z_H)=(0.073±0.075, −0.063±0.072) for humans and (x_H/z_H, y_H/z_H)=(0.081±0.034, −0.119±0.023) for guinea pigs. In the principal frame, (x'_H/z'_H, y'_H/z'_H)=(0.029±0.088, 0.039± 0.048) for humans and (x'_H/z'_H, y'_H/z'_H) =(−0.160±0.085, −0.019±0.031) for guinea pigs.
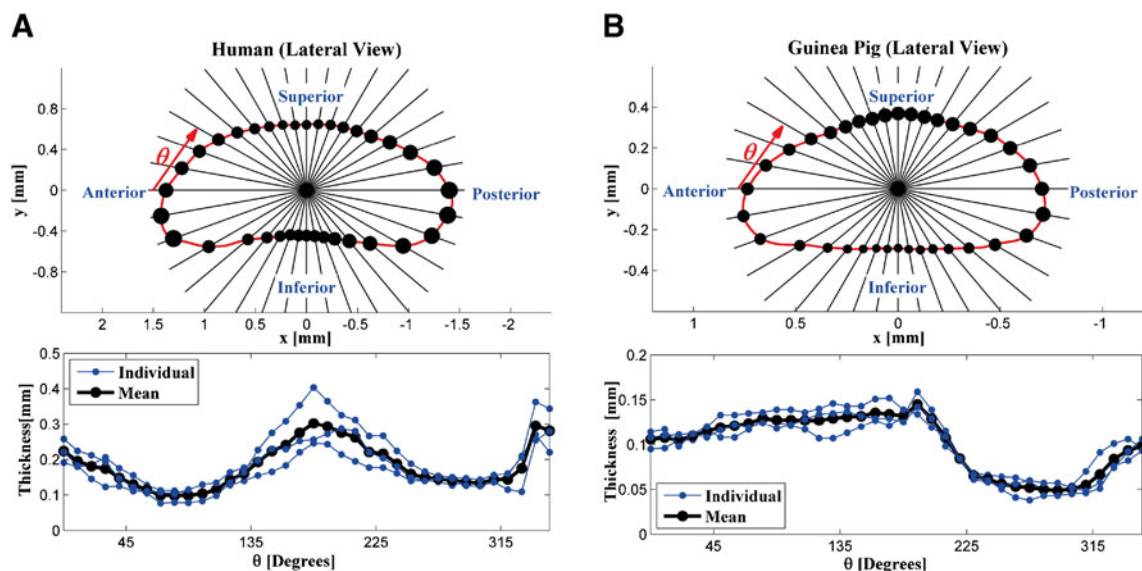
FIG. 9. Thickness map of the annular rim of the footplate measured in **A** three human and **B** three guinea pig stapes.

et al. 2008; Sim et al. 2010a, b; Eiber et al. 2012). While the classical "hinging motion" of the malleus–incus complex provides forces in the z direction on the stapes head, other possible modes of the malleus–incus complex motion at high frequencies are expected to transfer the forces in the x- and y-directions on the stapes head as well. When the same amounts of the rocking stimuli are acting on the stapes head, moments applied to the footplate of the stapes are proportional to its height. Therefore, the relatively large height of the human stapes is efficient to generate rocking-like motions of the stapes. Contrarily, for the reverse stimulation in which the cochlear fluid generates stimuli for motion of the stapes, the relatively large height of the human stapes is efficient to constrain the rocking-like motions because it needs relatively small constraint forces.

From a classical theory of vibration, inertial components of a rigid body provide inertial resistance to the corresponding motion components and effects of the inertias increase as frequency increases. In both human and guinea pig stapes, the principal moment of inertia of the stapes in the x'-axis was larger than the principal moment of inertia of the stapes in the y'-axis, indicating larger inertial resistance to the rocking-like motion along the long axis than inertial resistance to the rocking-like motion along the short axis of the footplate at high frequencies. In measurements of human stapes motion by Hato et al. (2003) and Sim et al. (2010a), the rocking-like motion along the short axis of the footplate was generally larger than the rocking-like motion along the long axis of the footplate at frequencies above 3 kHz, and it might be related to the difference in the inertial values between the two motion components.

All analyses about the effects of the anatomical features of the stapes on the rocking-like motions in this section are based on an assumption of the same amounts of stimuli on the stapes head for the two rocking-like motions. In reality, the direction and magnitude of the forces transmitted from the incus to the stapes in the frequency domain are determined

TABLE 4

Dependence of human stapes dimensions on gender (mean±standard deviation)

Symbol	Female (n=15)	Male (n=25)	p value
a [mm]	2.75±0.156	2.82±0.134	0.175
b [mm]	1.17±0.076	1.32±0.068	< 0.001
a/b	2.35±0.201	2.14±0.137	< 0.01
A_{FT} [mm^2]	2.76±0.251	3.17±0.225	< 0.001
A_{FT_proj} [mm^2]	2.59±0.223	2.99±0.204	< 0.001
d_{FT_eq} [mm]	1.87±0.086	2.01±0.071	< 0.001
$d_{FT\_eq\_proj}$ [mm]	1.81±0.079	1.95±0.067	< 0.001
h [mm][a]	3.28±0.25	3.27±0.173	
V_{ST} [mm^3][a]	1.25±0.141	1.47±0.144	

Mann–Whitney test was applied to comparison between female and male subjects

[a]Statistical calculation was not performed due to the limited number of the samples (n=5 for female and n=14 for male)
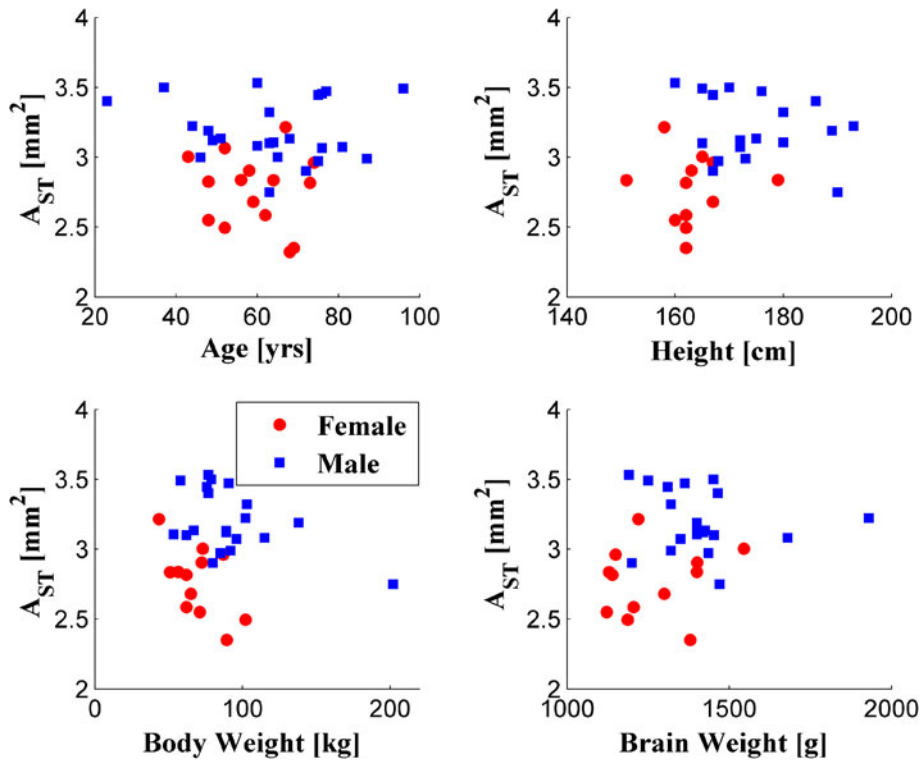
FIG. 10. Dependence of footplate area (medial surface) on age, height, body weight, and brain weight. The correlation of the footplate area with age, height, body weight, and brain weight was examined with linear regression, and the obtained p values were 0.646, 0.184, 0.737, and 0.157, respectively, indicating no significant correlation.

together with the mechanics of the eardrum and malleus–incus complex. Further, effects of the annular ligament of the stapes and cochlear fluid were not considered. As the thickness map of the annular rim of the footplate is different between the human and guinea pig stapes (Fig. 9), the annular ligament of the stapes footplate is presumed to provide different spatial stiffness in both species. More comprehensive analysis

TABLE 5

Comparison of human stapes dimension with data in the literature (mean±standard deviation)

Description	Symbol	Present data	Data in literatures	
			Value	Source
Long length of footplate	a [mm]	2.81±0.158	3.2	Stuhlman (1937)
			2.8	Arensburg et al. (1981)
			2.8	Weistenhöfer and Hudde (1999)
			2.57±0.33	Unur et al. (2002)
			2.5	Gan et al. (2002)
			3.3	Hato et al. (2003)
Short length of footplate	b [mm]	1.27±0.109	1.4	Stuhlman (1937)
			1.3	Arensburg et al. (1981)
			1.23	Weistenhöfer and Hudde (1999)
			1.29±0.22	Unur et al. (2002)
			1.4	Hato et al. (2003)
Footplate area	A_{FT} [mm^2]	3.03±0.331	3.2	Stuhlman (1937)
			2.97±0.25	Sim et al. (2010a, b)
Projected footplate area	A_{FT_proj} [mm^2]	2.86±0.316	3.85 (3.00–5.30)	Stenfelt et al. (2004)
Total height of the stapes	h [mm]	3.28±0.210	4	Stuhlman (1937)
			3.5	Bouchet and Giraud (1968)
			3.2	Arensburg et al. (1981)
			3.19±0.20	ÀWengen et al. (1995)
			3.5	Weistenhöfer and Hudde (1999)
			3.22±0.31	Unur et al. (2002)
Height of the center of the mass	h_c [mm]	1.22±0.157	1.3	Weistenhöfer and Hudde (1999)
Volume of the stapes	V_{ST} [mm^3]	1.43±0.242	1.44	Beer et al. (1999)
			1.44	Puria et al. (2007)

for the spatial mode patterns of the stapes motion in the frequency domain will be possible with a precise biomechanical model of the whole middle-ear structures, and this study provides the precise anatomical information of the stapes needed for this purpose.

The shapes of the footplate were also different between human and guinea pig. While the shape of the medial surface of the human stapes footplate was similar to the shape of a human foot, the medial surface in guinea pigs was oval-shaped. In human stapes, the shape of the medial surface from the right ears was similar to the shape of a left foot and the shape of the medial surface from the left ears was similar to the shape of a right foot. This distinctive shape of the medial surface in human stapes was also observed by Hagr et al. (2004). In addition, the shape like a big toe (Fig. 5A) was observed in 29 of the 53 human stapes. Thereby, whether a stapes was from a right or left ear could be identified by the shape of the medial surface of the footplate for the human stapes, but not for guinea pig.

In both human and guinea pig, the medial surface of the footplate was curved rather than flat. With such a nonflat shape of the surface, in-plane motions of the footplate along the footplate plane (i.e., x–y plane) may generate more fluid flow in the cochlea than fluid flow with a flat surface. The nonflat shape of the surface may also reduce fluid flux produced by the rocking-like motions, but the reduction is expected not to be considerably large because the rotational axes of the rocking-like motions are presumed to exist within or near the footplate (Hato et al. 2003; Lauxmann et al. 2012; Sim et al. 2010a, b) and the center of the medial surface curvatures far from the footplate. As different longitudinal arches of the medial surface of the footplate between human and guinea pig stapes were observed, the rocking-like motions of the stapes about the short axis of the footplate could produce different fluid flux in the cochlea.

Individual differences in the dimension of the stapes were larger for human than for guinea pigs. Such large individual differences were also found in other middle-ear anatomy (Sim and Puria 2008). The large individual difference observed in stapes motion (Hato et al. 2003; Sim et al. 2010a, b) might be related to the large individual difference in the middle-ear anatomy. However, considering the fact that improvement of hearing can be generally achieved by stapedectomy or stapedotomy for patients with various middle-ear anatomy and conditions, it is questionable whether the large individual difference in the middle-ear anatomy results in individual difference in hearing. These issues were beyond the scope of this study and would require additional investigation.

Asymmetric features of the stapes

Two asymmetric features of the stapes found in this study were (1) asymmetry of the stapes footplate with respect to the long axis (x-axis) of the footplate (Table 3) and (2) offset of the stapes head in the reference frame based on the medial surface of the footplate (intrinsic frame in this study). The two asymmetric features are dependent because the offset of the stapes head in the superior–inferior direction is related to the asymmetry of the stapes footplate with respect to the long axis of the footplate. In our previous study of the effects of the rocking-like motions on cochlear activation (Eiber et al. 2012), offset of the measurement point on the stapes head from the centroid of the medial surface of the footplate in guinea pigs was measured in the same manner as in this study and found to be 0.094± 0.031 mm to the anterior direction and 0.096± 0.019 mm to the inferior direction. Considering that the measurement point in the previous study was located on the superior part of the stapes head, the offset of the measurement point agrees with the results of this study (i.e., the center of the stapes head has an offset of 0.107±0.043 mm to the anterior direction and 0.157±0.027 mm to the inferior direction). In the study by Eiber et al. and many other studies on modeling of the stapes and cochlea, the rocking-like motion has been assumed to generate no net volume displacement at the oval window. The intrinsic frame introduced in this study is meaningful in the sense that rotational motions along the x- and y-axes do not produce net volume displacement at the oval window. Uncertainty of the measured rocking-like motion due to the offset of the stapes head were treated with possible error ranges of the obtained rocking-like motion in the study by Eiber et al. In this study, another reference frame was also introduced, the principal frame, which may be meaningful from the point of view of dynamics of the stapes.

In previous measurements and descriptions of spatial motions of the stapes (Decraemer et al. 2007; Eiber et al. 2012; Hato et al. 2003; Huber et al. 2008; Sim et al. 2010a), the reference frames were not clearly specified or alignment of the stapes in the reference frame was done imprecisely through a microscopic view. With a rough estimation of the reference frame or rough alignment of the stapes in the reference frame, the obtained spatial components of the stapes motion may differ considerably. Lauxmann et al. (2012) showed that the in-plane motions of the footplate in the human stapes were up to 20 % of the piston-like motion in their roughly estimated reference frame and could be minimized within 5 % of the piston-like motion in a plane, which is anatomically within the footplate. Now that the asymmetry of the stapes has been documented, the reference frame should be specified when the spatial motion of the stapes is described.

Gender differences in human stapes

A prominent finding in this study was that the shape and size of the human stapes footplate is dependent on gender. The ratio of the short length to the long length of the footplate in male subjects was larger than the corresponding value in female subjects, together with a larger footplate area in the male subjects. With such differences, the physiological motions of the stapes in female and male subjects might be different. However, while age-associated hearing loss was reported to be larger in men (Pearson et al. 1995), no significant difference of hearing between young (<30 years) men and women has been reported (ISO 7029; International Organization for Standardization 2000; Stenklev and Laukli 2004). Simulating how these anatomical differences affect the physiological motions of the stapes and, thus, hearing requires a sophisticated model including other middle-ear and inner-ear anatomy. This may be an important future direction but is not within the scope of this study.

The shape and size of the human stapes footplate did not depend on other subject data, such as age, height, body weight, and brain weight.

CONCLUSION

The primary aim of this study was to provide precise information about the shapes and dimensions of the stapes in human and guinea pigs. The height of the stapes relative to the footplate size in the human stapes was found to be larger than the corresponding value in guinea pig. In both human and guinea pig stapes, the footplate was asymmetric with respect to the long axis and the location of the stapes head had an offset in the reference frame based on the medial surface of the footplate, indicating the necessity to include the exact description of the reference frame in characterizing stapes motion. The medial surface of the footplate was found to be curved rather than flat. A further aim of the study was to determine if stapes characteristics varied as a function of subject. An association of gender with stapes dimensions was determined.
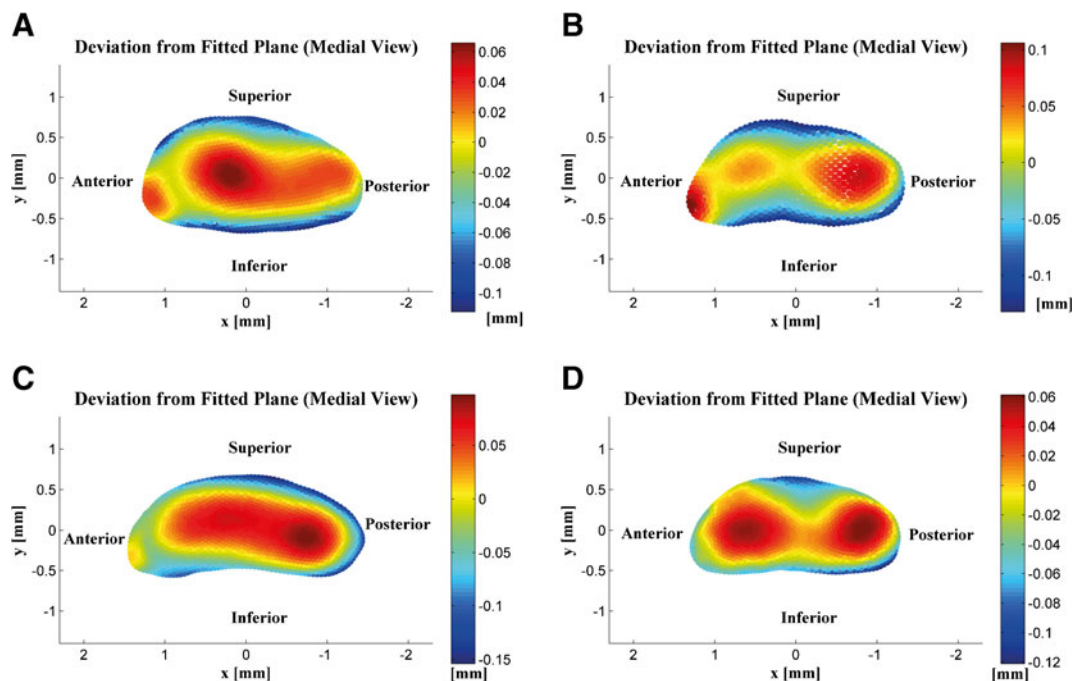
ACKNOWLEDGMENTS

APPENDIX

FIG. 11. Four types of the medial surfaces of the footplate that are different from the general profiles of the medial surface. **A** Nonobvious medial peak in the posterior region, **B** nonobvious medial peak in the anterior region, **C** a small or nonobvious lateral peak around the center of the surface, and **D** no protruding at the anterior inferior edge.

REFERENCES

Aʀᴇɴsʙᴜʀɢ B, Hᴀʀᴇʟʟ M, Nᴀᴛʜᴀɴ H (1981) The human middle ear ossicles, morphometry and taxonomic implications. J Hum Evol 10:199–205

Àᴡᴇɴɢᴇɴ DF, Kᴜʀᴏᴋᴀᴡᴀ H, Nɪsʜɪʜᴀʀᴀ S, Gᴏᴏᴅᴇ RL (1995) Measurements of the stapes superstructure. Ann Otol Rhinol Laryngol 104:311–316

Bᴇᴇʀ HJ, Bᴏʀɴɪᴛᴢ M, Hᴀʀᴅᴛᴋᴇ HJ, Sᴄʜᴍɪᴅᴛ R, Hᴏғᴍᴀɴɴ G, Vᴏɢᴇʟ U, Zᴀʜɴᴇʀᴛ T, Hüᴛᴛᴇɴʙʀɪɴᴋ KB (1999) Modelling of components of the human middle ear and simulation of their dynamic behaviour. Audiol-Neurootol 4:156–162

Bᴏᴜᴄʜᴇᴛ A, Gɪʀᴀᴜᴅ M (1968) Contribution a l'etude morphologique et radiologique des osselets de l'ouie. Compte rendu de l' Association des Anatomists 53 Congrés 141:588–600

Bᴜʏᴛᴀᴇʀᴛ JA, Sᴀʟɪʜ WH, Dɪᴇʀɪᴄᴋ M, Jᴀᴄᴏʙs P, Dɪʀᴄᴋx JJJ (2011) Realistic 3D computer model of the gerbil middle ear, featuring accurate morphology of bone and soft tissue structures. J Assoc Res Otolaryngol 12(6):681–696

Dᴇᴄʀᴀᴇᴍᴇʀ WF, Kʜᴀɴɴᴀ SM, Fᴜɴɴᴇʟʟ WRJ (2000) Measurement and modeling of the three-dimensional vibration of the stapes in cat. In: Wada H, Takasaka K, Ikeda K, Phyama K, Koike T (eds) Proceeding of the Symposium on Recent Developments in Auditory Mechanics. World Scientific, Singapore, pp 36–43

Dᴇᴄʀᴀᴇᴍᴇʀ WF, Dɪʀᴄᴋx JJJ, Fᴜɴɴᴇʟ WRJ (2003) Three-dimensional modeling of the middle-ear ossicular chain using a commercial high-resolution X-ray CT scanner. JARO 04:250–263

Dᴇᴄʀᴀᴇᴍᴇʀ WF, ᴅᴇ Lᴀ Rᴏᴄʜᴇғᴏᴜᴄᴀᴜʟᴅ O, Dᴏɴɢ W, Kʜᴀɴɴᴀ SM, Dɪʀᴄᴋx JJ, Oʟsᴏɴ ES (2007) Scala vestibuli pressure and three-dimensional stapes velocity measured in direct succession in gerbil. J Acoust Soc Am 121(5):2774–2791

Eɪʙᴇʀ A (1999) Mechanical modeling and dynamical behavior of the human middle ear. Audiol Neurootol 4:170–177

Eɪʙᴇʀ A, Hᴜʙᴇʀ AM, Lᴀᴜxᴍᴀɴɴ M, Cʜᴀᴛᴢɪᴍɪᴄʜᴀʟɪs M, Sᴇǫᴜᴇʀɪᴀ D, Sɪᴍ JH (2012) Contribution of complex stapes motion to cochlea activations. Hear Res 284:82–92

Eʟᴋʜᴏᴜʀɪ N, Lɪᴜ H, Fᴜɴɴᴇʟʟ WRJ (2006) Low-frequency finite-element modeling of the gerbil middle ear. J Assoc Res Otolaryngol 7:399–411

Fᴀʀᴀʜᴀɴɪ RM, Nᴏᴏʀᴀɴɪᴘᴏᴜʀ M (2008) Anatomy and anthropometry of human stapes. Am J Otolaryngol 29(1):42–47

Fᴜɴɴᴇʟʟ WRJ (1984) On the calculation of surface areas of objects reconstructed from serial sections. Journal of Neuroscience Methods 11:205–210

Gᴀɴ RZ, Sᴜɴ Q, Dʏᴇʀ RK Jʀ, Cʜᴀɴɢ KH, Dᴏʀᴍᴇʀ KJ (2002) Three-dimensional modeling of middle ear biomechanics and its applications. Otology & Neurotology 23:271–280

Gᴀɴ RZ, Rᴇᴇᴠᴇs BP, Wᴀɴɢ X (2007) Modeling of sound transmission from ear canal to cochlea. Ann Biomed Eng 35(12):2180–2195

Hᴀɢʀ AA, Fᴜɴɴᴇʟʟ RJ, Zᴇɪᴛᴏᴜɴɪ AG, Rᴀᴘᴘᴀᴘᴏʀᴛ JM (2004) High-resolution X-ray CT scanning of the human stapes footplate. J Otolaryngol 33(4):217–221

Hᴀᴛᴏ N, Sᴛᴇɴғᴇʟᴛ S, Gᴏᴏᴅᴇ RL (2003) Three-dimensional stapes footplate motion in human temporal bones. Audiology & Neuro-Otology 8:140–152

Hᴜʙᴇʀ AM, Sᴇǫᴜᴇɪʀᴀ D, Bʀᴇᴜɴɪɴɢᴇʀ C, Eɪʙᴇʀ A (2008) The effects of complex stapes motion on the response of the cochlea. Otol Neurotol 29(8):1187–1192

Iɴᴛᴇʀɴᴀᴛɪᴏɴᴀʟ Oʀɢᴀɴɪᴢᴀᴛɪᴏɴ ғᴏʀ Sᴛᴀɴᴅᴀʀᴅɪᴢᴀᴛɪᴏɴ (2000) Acoustics—statistical distribution of hearing thresholds as a function of age, ISO 7029:2000(E). ISO, Geneva

Iʏᴇʀ PV, Gʀɪsᴛᴡᴏᴏᴅ RE (1984) Histopathology of the stapes in otosclerosis. Pathology 16(1):30–38

Jᴏʜɴs HE, Cᴜɴɴɪɴɢʜᴀᴍ JR (1974) The physics of radiology (3rd edition). Thomas, Springfield, IL

Kᴏɪᴋᴇ T, Wᴀᴅᴀ H, Kᴏʙᴀʏᴀsʜɪ T (2002) Modeling of the human middle ear using the finite element method. J Acoust Soc Am 111(3):1306–1317

Lᴀɴᴇ JI, Wɪᴛᴛᴇ RJ, Hᴇɴsᴏɴ OW, Dʀɪsᴄᴏʟʟ CLW, Cᴀᴍᴘ J, Rᴏʙʙ RA (2005) Imaging microscopy of the middle and inner ear: Part II: MR microscopy. Clinical Anatomy 18:409–415

Lᴀᴜxᴍᴀɴɴ M, Eɪʙᴇʀ A, Hᴇᴄᴋᴇʟᴇʀ C, Iʜʀʟᴇ S, Cʜᴀᴛᴢɪᴍɪᴄʜᴀʟɪs M, Hᴜʙᴇʀ AM, Sɪᴍ JH (2012) In-plane motion of the stapes in human ears. J Acoust Soc Am 132(5):3280–3291

Mᴀᴄᴏᴠsᴋɪ A (1983) Medical image system. Prentice-Hall Inc., Upper Saddle River, NJ

Mᴇʀᴄʜᴀɴᴛ SN, Iɴᴄᴇsᴜʟᴜ A, Gʟʏɴɴ RJ ᴇᴛ ᴀʟ (2001) Histologic studies of the posterior stapediovestibular joint in otosclerosis. J Otology & Neurotology 22(3):305–310

Nᴀᴅᴏʟ JB (2001) Histopathology of residual and recurrent conductive hearing loss after stapedectomy. J Otology & Neurotology 22 (2):162–169

Pᴇᴀʀsᴏɴ JD, Mᴏʀʀᴇʟʟ CH, Gᴏʀᴅᴏɴ-Sᴀʟᴀɴᴛ S, Bʀᴀɴᴛ LJ, Mᴇᴛᴛᴇʀ EJ, Kʟᴇɪɴ LL, Fᴏᴢᴀʀᴅ JL (1995) Gender differences in a longitudinal study of age-associated hearing loss. Acoust Soc Am 97(2):1196–1205

Pᴜʀɪᴀ S, Sᴛᴇᴇʟᴇ C (2010) Tympanic membrane and malleus–incus-complex co-adaptations for high-frequency hearing in mammals. Hear Res 263:183–190

Pᴜʀɪᴀ S, Sɪᴍ JH, Sʜɪɴ M, Tᴜᴄᴋ-Lᴇᴇ J, Sᴛᴇᴇʟᴇ CR (2007) Middle ear morphometry from cadaveric temporal bone micro-CT imaging. In: Huber A and Eiber A (eds) Middle ear mechanics in research and otology, World Scientific Press, Singapore, pp 259–268

Rᴏsᴏᴡsᴋɪ JJ, Mᴇʀᴄʜᴀɴᴛ SN (1995) Mechanical and acoustical analysis of middle ear reconstruction. The American Journal of Otology 16(4):486–497

Sᴀʀʀᴀᴛ R, Tᴏʀʀᴇs A, Gᴜᴢᴍᴀɴ AG, Lᴏsᴛᴀʟᴇ F, Wʜʏᴛᴇ J (1992) Functional structure of human auditory ossicles. Acta Anat 144 (3):189–195

Sɪᴍ JH, Pᴜʀɪᴀ S (2008) Soft tissue morphometry of the malleus–incus complex from micro-CT imaging. J Assoc Res Otolaryngol 9:5–21

Sɪᴍ JH, Pᴜʀɪᴀ S, Sᴛᴇᴇʟᴇ CR (2007) Calculation of the inertial properties of the malleus–incus complex from micro-CT imaging. J Mech Mater Struct 2(8):1515–1524

Sɪᴍ JH, Cʜᴀᴛᴢɪᴍɪᴄʜᴀʟɪs M, Lᴀᴜxᴍᴀɴɴ M, Röösʟɪ C, Eɪʙᴇʀ A, Hᴜʙᴇʀ AM (2010ᴀ) Complex stapes motions in human ears. J Assoc Res Otolaryngol 11(3):329–341

Sɪᴍ JH, Cʜᴀᴛᴢɪᴍɪᴄʜᴀʟɪs M, Lᴀᴜxᴍᴀɴɴ M, Röösʟɪ C, Eɪʙᴇʀ A, Hᴜʙᴇʀ AM (2010ʙ) Errors in measuring three-dimensional motions of the stapes using a laser Doppler vibrometer system. Hear Res 270:4–14

Sᴛᴇɴғᴇʟᴛ S, Hᴀᴛᴏ N, Gᴏᴏᴅᴇ RL (2004) Fluid volume displacement at the oval and round windows with air and bone conduction stimulation. J Acoust Soc Am 115:797–812

Sᴛᴇɴᴋʟᴇᴠ NC, Lᴀᴜᴋʟɪ E (2004) Presbyacusis—hearing thresholds and the ISO 7029. Int J Audiol 43(5):295–306

Sᴛᴜʜʟᴍᴀɴ O (1937) The nonlinear transmission characteristics of the auditory ossicles. J Acoust Soc Am 9:119–128

Uɴᴜʀ E, Üʟɢᴇʀ H, Eᴋíɴᴄɪ N (2002) Morphometrical and morphological vibrations of middle ear ossicles in the newborn. Erciyes Medical Journal 24(2):57–63

Vᴏɪᴇ AH, Bᴜʀɴs DH, Sᴘᴇʟᴍᴀɴ FA (1993) Orthogonal-plane fluorescence optical sectioning: three-dimensional imaging of biological specimens. J Microsc 170(3):229–236

Wᴇɪsᴛᴇɴʜöғᴇʀ C, Hᴜᴅᴅᴇ H (1999) Determination of the shape and inertia properties of the human auditory ossicles. Audiology & Neuro-Otology 4:192–196

Wᴇᴠᴇʀ E, Lᴀᴡʀᴇɴᴄᴇ M (1954) Physiological acoustics. Princeton University Press, Princeton

Wʏsᴏᴄᴋɪ J, Sʜᴀʀɪғɪ M (2005) Measurements of selected parameters of the guinea pig temporal bone. Folia Morphol 64(3):145–150